Int J Adv Manuf Technol (2017) 92:569–581
DOI 10.1007/s00170-017-0097-4

ORIGINAL ARTICLE

Comparison between IEF model and numerical method based on the derivation method of Bridgman to evaluating fracture toughness in galvanized steel sheet

Lotfi Daoud[1] · **Abdelaziz Belhamzaoui**[2] · **Abdelaziz Amirat**[1]

Received: 15 October 2016 / Accepted: 23 January 2017 / Published online: 1 March 2017

Abstract The present work proposes a new numerical approach based on the derivation method of Bridgman to determine (K_{IC}) of galvanized steel sheets. The method relies on a fracture analysis numerical code "Franc2D," which permits to simulating the initiation and propagation of a crack on grooved tensile specimens. First, the stress intensity factor is obtained while the crack is propagating and then (K_{IC}) is determined from the fitting curves of the stress intensity factor (K_I) to crack length (a) plot through mathematical transformations. The results are validated by comparing them to those obtained through the experimental approach using Vickers hardness based *IEF* engineering models. The relative values of (K_{IC}) are admissible and acceptable with a coefficient of variation of 14% for a large range of groove radius. Hence, the present numerical simulation can be fairly used in order to reduce time consuming and avoid costly experimental mechanical tests.

Keywords Vickers hardness · Tensile testing · Fracture toughness (K_{IC}) · Triaxiality · *IEF* model · Franc2D

✉ Lotfi Daoud
lotfi.daoud@univ-annaba.org

Abdelaziz Belhamzaoui
a_belhamzaoui@yahoo.fr

Abdelaziz Amirat
abdelaziz.amirat@univ-annaba.dz

[1] Research Laboratory of Advanced Technology in Mechanical production (LRTAPM), Department of Mechanical Engineering, Faculty of Engineering Sciences, Badji Mokhtar University Annaba, 12-23000 Annaba, BP, Algeria

[2] Mechanics of Materials and Plant Maintenance Research Laboratory (LR3MI), Department of Mechanical Engineering, Faculty of Engineering Sciences, Badji Mokhtar University Annaba, 12-23000 Annaba, BP, Algeria

Nomenclature

A	Material yield parameter (MPa)
a	Crack length (mm)
a_c	Critical crack length (mm)
B	Width of the smooth tensile test specimen before fracture (mm)
CASCA	Mesh generator for "Franc2D"
CVN	Charpy V-Notch
D	Indenter diameter (mm)
d	Arithmetic mean of the two diagonals of the indentation (mm)
d_1, d_2	Averages diameters of two diagonals of indentation (mm)
E	Young's modulus (MPa)
$f(a)$	Function that describes the relationship between stress intensity factor and crack length
Franc2D	(MPa $m^{1/2}$)
GeoGebra	Fracture analysis code. Free mathematical software
h	Penetration depth for Vickers hardness test (mm)
H_v	Vickers hardness (kgf/mm^2)
HDG	Hot-dip-galvanized
IEF	Indentation energy to fracture
k	Parameter of Meyer test
K	Strength coefficient exponent of the Hollomon-type flow curve
K_I	Stress intensity factor in mode 1 (MPa $m^{1/2}$)
K_{IC}	Fracture toughness (MPa $m^{1/2}$)
K_{ICLS}	Lower shelf of the fracture toughness for ferritic steel (MPa $m^{1/2}$)
m	Meyer index
n	Work-hardening exponent of the Hollomon-type flow curve
P	Applied load in the hardness test (N)
p_m^f	Critical mean contact pressure (MPa)

R	Radius of curvature of the neck after fracture (mm)
R_i	Curvature radius for a given flat specimen (mm)
RPV	Reactor pressure vessel
r	The specimen half width at curvature after fracture (mm)
r_0	The specimen half width at curvature before fracture (mm)
S	Slope of the linear load (P)-penetration depth (h) (N/mm)
SIG Y	Stress in Y direction obtained by "Franc2D" software (ksi) or (MPa)
t_0	Thickness of the tensile test specimen before fracture (mm)
t	Thickness of the tensile test specimen after fracture (mm)
t_f	Stress triaxiality in tensile test
t_f^{ID}	Stress triaxility for indentation deformation
w_0	Initial width of specimen at curvature before fracture (mm)
w	Final width of specimen at curvature after fracture (mm)
W_0	Lower shelf fracture energy (J/m^2)
λ	Material constant for fracture strain and stress triaxiality
α	Material constant for fracture strain and stress triaxiality
ν	Poisson's ratio
ε_f	Fracture strain
ε_{xx}, ε_{yy}, ε_{zz}	Deformations in three directions
ε_u	True ultimate strain
σ	Applied stress (MPa)
σ_e	Yield stress (MPa)
σ_{eq}	Von Mises equivalent stress (MPa)
σ_h	Hydrostatic stress (MPa)
σ_{xx}, σ_{yy}, σ_{zz}	Stress in three directions (MPa)
σ_u	True ultimate stress (MPa)

1 Introduction

Galvanized steel sheets are widely used in civil construction and engineering applications requiring corrosion protection such as highway drainage culverts and automotive industry where formability and weldability are involved [1]. However, the corrosion process is unpredictable and can take place in the galvanized steel and eventually generates cracks that may grow up to material failure. Therefore, much research work of the crack behavior in galvanized steel sheet is investigated [2–7].

Nowadays, investigations are oriented to the understanding of the behavior of the corrosion mechanism in galvanized steel sheets in order to assess their lifetime through the material mechanical properties and fracture mechanics concepts. Coni et al. have evaluated how much coating influences the mechanical properties on steel sheet. For instance, when coated with zinc alloy (55% Al-Zn), the specific yield and tensile strengths are higher and the total elongation and hardening coefficient are lower compared to the galvanized sheets [1]. Kim et al. have investigated the effects of galling, a form of adhesive wear employed on die to stamp automotive components made of advanced high strength steel in order to reduce die maintenance cost and scrap rate [8]. Ploypech et al. have analyzed the fracture behavior of galvanized steels using four point bending specimens in order to characterize and simulate numerically the evolution of crack from the initiation to propagation stages. Crack initiation started near the steel-coating layer interface and propagated toward the outer coating layers [9]. Lai et al. have provided computational solutions in order to estimate the fatigue live for adhesive-bonded lap-shear specimens. These have been applied on magnesium alloy (AZ31) and hot-dip-galvanized (HDG) mild steel sheets with and without kinked cracks on the basis of kinked crack growth model and material constant for the Paris law [10].

Usually, experimental methods are known as destructive, time consuming, and costly; therefore, researchers have attempted to estimate the fracture analyses using faster and less destructive techniques. The indentation energy to fracture (IEF) method has been proposed by Byun et al. in order to estimating the fracture toughness of ferritic *RPV* steels. The methodology has been applied to determine the relationships between the stress state and the fracture parameters in the fracture toughness transition region. The critical fracture stresses were obtained by considering the stress triaxiality for the crack tip [11]. The IEF method based on automated ball

Table 1 Chemical composition of the galvanized E26 steel sheet, in weight %

Grade steel	Chemical composition, w_t%										
E26	C	Mn	P	S	Si	Cr	Mo	Cu	Ni	N	Al
	0.08	0.36	0.006	0.003	0.002	0.024	0.003	0.023	0.021	0.0086	0.029

Table 2 Specific mechanical properties of the galvanized E26 steel sheet

Grade steel	Maximum yield strength	Tensile strength	Minimum elongation
E26	300 MPa	270 to 410 MPa	28%

indentation is nowadays commonly employed to evaluate material fracture toughness [12–14].

The substitution ball indenter for Vickers indenter has been proposed by of Mohammadi et al. They have predicted fracture toughness values of (3Cr-1Mo) steel from Vickers indentation and tensile test data using (*IEF*) model. Comparing to Charpy V-Notch (CVN) impact test results, the relative results were in good agreement [15].

In the present work, the fracture toughness of galvanized E26 steel sheet has been investigated using numerical method based on free fracture analysis code distributed by Cornell University, Franc2D. To validate the numerical analysis, results are compared to those obtained by the IEF model where the fracture toughness is calculated through the determination of stress triaxiality and Vickers hardness values. The aim of the present paper is to contribute in optimizing the determination of fracture toughness of galvanized steel sheet through numerical solution based on the derivation method of Bridgman.

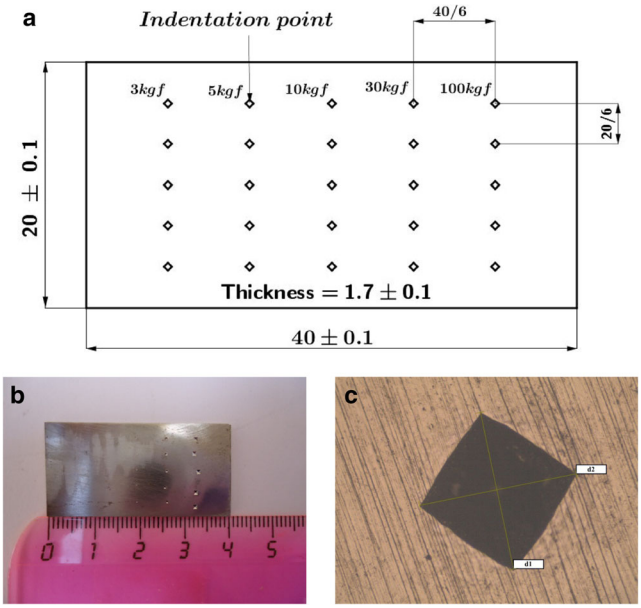

Fig. 1 **a** Schematic repartition of the indentations points in the galvanized E26 steel sheet. **b** Hardness test specimen. **c** 200-fold enlargement of an indentation

Table 3 Geometric parameters for Vickers hardness test under applied load

Geometrical model	Formula
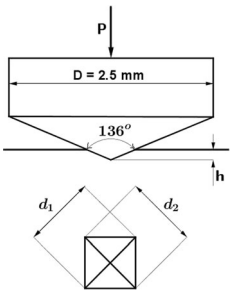	$a)\ Hv = 2sin\left(\frac{136^{\circ}}{2}\right)\ \frac{P}{d^2} \simeq 1.8544\ \frac{P}{d^2}$ b) $d = \frac{d_1+d_2}{2}$ c) $h = \frac{d}{2\sqrt{2}\tan(68^{\circ})} \simeq \frac{d}{7}$ With H_v: Vickers hardness P: Applied load D: Diameter of diamond pyramid = 2.5 mm d_1, d_2: Two diagonals of the indentation d: Arithmetic mean of two diagonals h: Penetration depth

Table 4 Results of Vickers hardness tests on the galvanized E26 steel sheet

Test	D (mm)	P (kgf)	P (N)	d_1 (mm)	d_2 (mm)	d (mm)	h (mm)	Hv
1	2.5	3	29.41	0.2057	0.2009	0.2033	0.0290	134.64
2	2.5	5	49.02	0.2631	0.2519	0.2575	0.0368	139.94
3	2.5	10	98.04	0.3709	0.3657	0.3683	0.0526	137.02
4	2.5	30	294.12	0.6621	0.6576	0.6599	0.0943	127.72
5	2.5	100	980.39	1.2440	1.2326	1.2383	0.1769	120.86

2 Material

Galvanized E26 steel sheet, according to standards "NF EN 10130 edition April 2007," produced by cold rolling mill "LAF" unit of the steel complex El-Hadjar, Algeria, is used. The chemical composition and the specific mechanical properties are given in Tables 1 and 2.

3 Experimental procedures

Mechanical properties of the material are required when conducting numerical simulation under Franc2D code, and Vickers hardness values and the stress triaxiality of the material are used to calculate fracture toughness through "IEF model." So, the experimental procedures consist in carrying

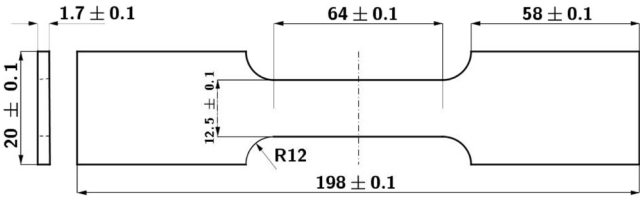

Fig. 2 Standard "ASTM E8" tensile specimen

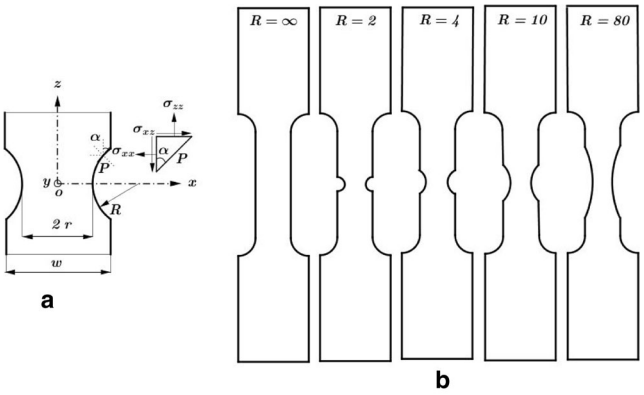

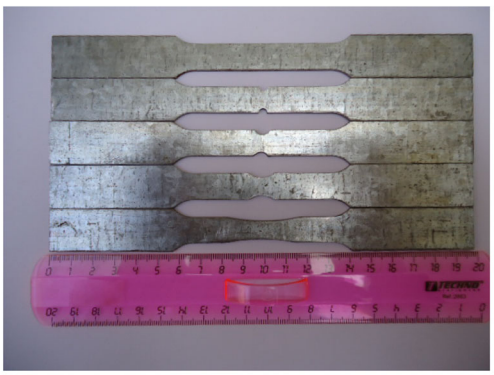

Fig. 3 **a** The cross section of flat grooved plane stress specimen after fracture. **b** Shape of the grooved specimens according to the radius *R*. **c** Smooth and grooved specimens

out tensile tests on standard specimens and grooved specimens and also exploratory Vickers indentation tests that are described below:

3.1 Hardness test

Vickers hardness tests have been carried out on a "Zwick/Roell-Zhu 8/187.5" universal hardness machine according to standards (ASTME92). A sample of (40 × 20) mm^2 × 1.7 mm thickness has been prepared from galvanized E26 steel sheet and then polished. Figure 1 shows the repartition of the indentation points on the sample. Five loads ranging from 3 to 100 kgf have been applied and five measurements have been recorded to check the reproducibility of the results.

The hardness values have been computed according to the formulations given in Table 3, and the corresponding results are given in Table 4.

Table 5 Parameter of the Hollomon-type flow curve

Parameter	*K* (MPa)	*n*	σ_u (MPa)	ε_u	σ_e (MPa)	*E* (GPa)	ν
Values	618.95	0.165	458.30	0.165	293	210	0.3

3.2 Standard and derivation method of Bridgman tensile tests

Tensile tests have been carried out on a "Zwick/Roell Z050" testing machine following the derivation method of Bridgman [16] and Bai [17] in order to determine the triaxiality of the material. Smooth tensile specimen blanks have been prepared from galvanized E26 steel sheet in the direction of the rolling process and then machined on universal milling machine according to standard "ASTM E8" (Fig. 2).

Then, according to derivation method of Bridgman, a series of specimen have been machined in the center of the gauge length as to get grooves of different sizes. This has been achieved by giving symmetrical curvature of a required radius using a corresponding mill cutter diameter. There should be noted that in all grooved specimens the initial width of (B = 12.5 mm) is reduced by the grooving process and is noted as follows: $w_0 = 2\ r_0 \simeq 8.5$ mm).

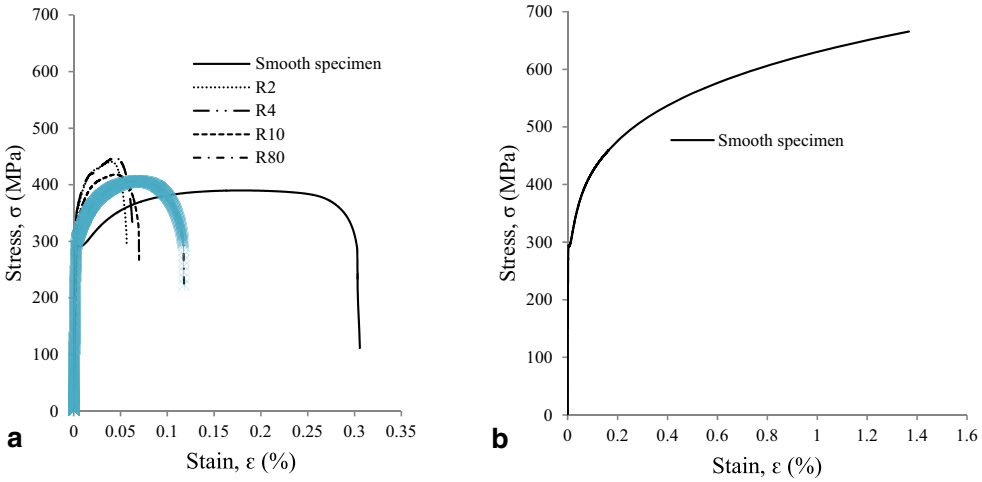

Fig. 4 Stress-strain curves. **a** Engineering. **b** True

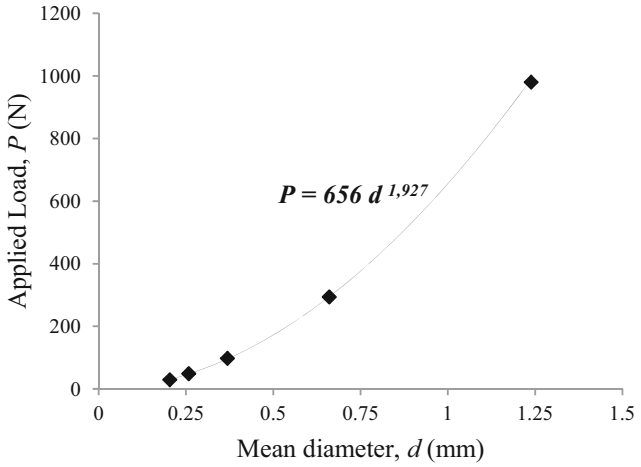

Fig. 5 Load-indentation diameter curve from Vickers tests

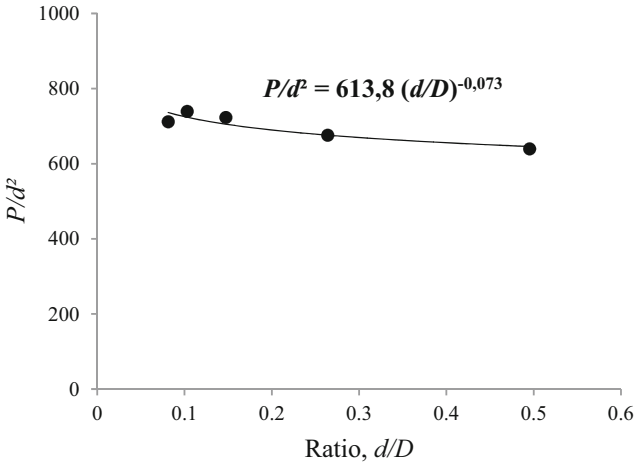

Fig. 7 Relationship between the indentation parameters

Figure 3 shows the geometry of a flat grooved specimen and the free plane stress body diagram [17] and illustrates the four geometries of specimen at the neck zone after fracture.

The true stress-strain curve is obtained from the engineering stress strain curve according to Hollomon law [18], Eq. (1):

$$\sigma = K\,\varepsilon^{n} \tag{1}$$

K and n are, respectively, the strength coefficient exponent and the work-hardening exponent of the *Hollomon-type* flow curve obtained from the engineering stress-strain curve for smooth specimen (Fig. 4). Table 5 summarizes the mechanical properties of the galvanized E26 steel sheet.

4 IEF model for K_{IC} determination

The analytical solution for determining fracture toughness (K_{IC}) is based on IEF engineering model, which is developed in the following steps: determining the parameters of IEF model from hardness and tensile tests, computing the stress triaxiality factor, and finally calculating the fracture toughness.

4.1 Determination of IEF model parameters from Vickers hardness and tensile tests

In the present work, the Vickers indentation and tensile test data have been used to determine the IEF engineering model as suggested by Mohammadi et al. [15] in order to estimate fracture toughness of galvanized E26 steel sheet, Eq. (2):

$$K_{IC} = \left[\frac{2\,E}{1-\nu^2}\left(W_0 + \frac{A^2\,D^2}{S}\left(\frac{p_m^f}{2\,A}\right)^{(2m-2)/(m-2)}\right)\right]^{\frac{1}{2}} \tag{2}$$

W_0 is the lower shelf fracture energy, Eq. (3):

$$W_0 = \frac{(K_{\mathrm{ICLS}})^2}{2\,E/(1-\nu^2)} \tag{3}$$

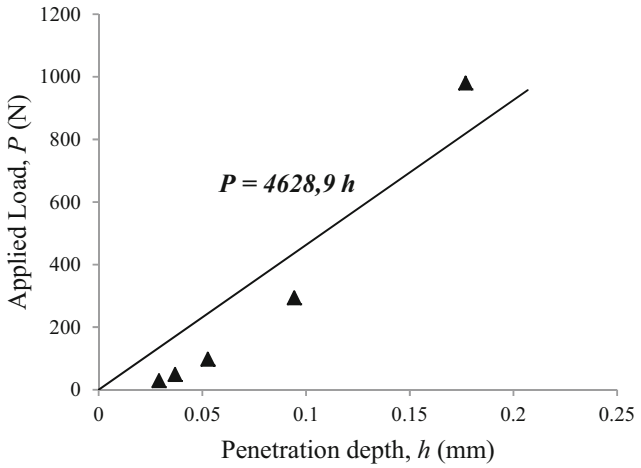

Fig. 6 Load-penetration depth curve from Vickers test data

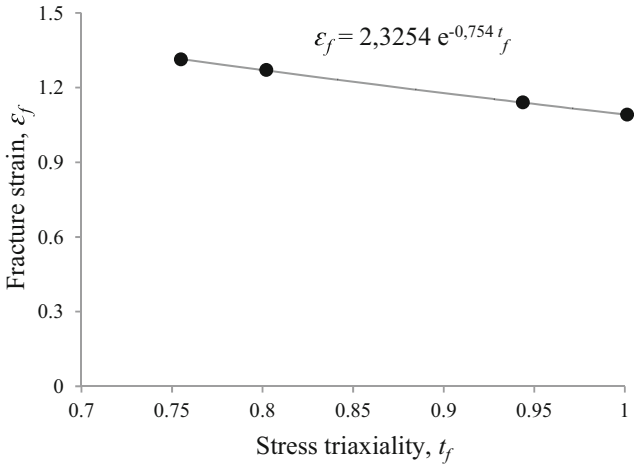

Fig. 8 Fracture strain to stress triaxiality curve

Table 6 Geometric data for stress triaxiality to fracture

Groove radius	R_i (mm)	R (mm)	w_0 (mm)	w (mm)	r (mm)	t_f
R_2	2	3.1	8.5	7.2	3.6	0.758
R_4	4	4.2	8.6	7.2	3.6	0.802
R_{10}	10	15.3	8.5	6.6	3.3	0.935
R_{80}	80	91.4	8.5	5.8	2.9	0.990

Table 7 Geometric data for fracture strain

Groove radius	w_0 (mm)	w (mm)	t_0 (mm)	t (mm)	ε_{xx}	ε_{yy}	ε_{zz}	ε_f
R_2	8.5	7.2	1.76	0.62	−0.166	−1.043	1.209	1.311
R_4	8.6	7.2	1.77	0.65	−0.178	−1.002	1.179	1.272
R_{10}	8.5	6.6	1.79	0.77	−0.253	−0.844	1.097	1.148
R_{80}	8.5	5.8	1.78	0.88	−0.382	−0.704	1.087	1.102

K_{ICLS} is the lower shelf of the fracture toughness for ferritic steel equals to 30 MPa $m^{1/2}$, as suggested in the literature [19].

The value of the lower shelf fracture energy W_0 is then 1950 J/m.

m is the Meyer index given in the Meyer law [20], Eq. (4):

$$P = k\, d^m \tag{4}$$

k is a coefficient in the Meyer law. m and k are determined from the plot of the applied load versus the indentation diameter of the Vickers test (Fig. 5) The corresponding values of k = 656 and m = 1.927 are deduced from the fitting curve power equation. According to Onitsch [21], the material is soft since $m > 1.6$.

S is the slope of the load-depth indentation curve (Fig. 6), and expressed by Eq. (5):

$$P = S\, h \tag{5}$$

The value of the slope (S) is then 4628.9 N/mm.

A is the material yield parameter for the fitting curve of the plot of (P/d^2) versus (d/D) (Fig. 7) and expressed in Eq. (6) by fitting the data to Meyer law:

$$\frac{P}{d^2} = A\left(\frac{d}{D}\right)^{m-2} \tag{6}$$

The value of A is then 613.8 MPa.

The critical mean contact pressure (p_m^f) is calculated using Eq. (7):

$$p_m^f = \left(t_f^{ID} + \frac{2}{3}\right) K\, \alpha^n\, e^{-\lambda\, n\, t_f^{ID}} \tag{7}$$

t_f^{ID} is the stress triaxility for indentation deformation expressed in Eq. (8):

$$t_f^{ID} = \frac{2\,A\,5^n}{K} - \frac{2}{3} \tag{8}$$

K and n are, respectively, the strength coefficient exponent and the work-hardening exponent of the Hollomon-type flow curve [18] obtained from the true stress-strain curve (Fig. 4 and Table 5).

α is a temperature-dependent parameter, and λ is a material constant determining the stress triaxiality-dependence fracture strain. The values of α and λ are determined from the fitting curve of the plot of the fracture strain ε_f versus the stress triaxility t_f obtained from the tensile tests [18, 17], expressed by an exponential Eq. (9) (see Fig. 8):

$$\varepsilon_f = \alpha\, e^{-\lambda\, t_f} \tag{9}$$

4.2 The stress triaxiality factor

The stress triaxiality factor (t_f) is given in Eq. (10) as the ratio of the hydrostatic stress (σ_h) and Von Mises equivalent stress (σ_{eq}):

$$t_f = \frac{\sigma_h}{\sigma_{eq}} \tag{10}$$

where σ_h and σ_{eq} are expressed in Eqs. (11) and (12):

$$\sigma_h = \frac{1}{3}\left(\sigma_{xx} + \sigma_{yy} + \sigma_{zz}\right) \tag{11}$$

$$\sigma_{eq} = \sqrt{\frac{1}{2}\left(\left(\sigma_{xx} + \sigma_{yy}\right)^2 + \left(\sigma_{yy} + \sigma_{zz}\right)^2 + \left(\sigma_{zz} + \sigma_{xx}\right)^2\right)} \tag{12}$$

In the non-deformed state and using the geometric parameters (Fig. 3), the triaxiality factor for sheet specimens in the symmetry plane of the neck, t_f, is given in Eq. (13) [16, 22]:

$$t_f = \left[\left(1 + \frac{2R}{r}\right)^{1/2} ln\left(1 + \frac{r}{R} + \left(\frac{2r}{R}\right)^{1/2}\left(1 + \frac{r}{2R}\right)^{1/2}\right) - 1\right]^{-1} \tag{13}$$

Table 8 K_{IC} result from the IEF model

Parameter	E (GPa)	ν	n	K (MPa)	m	W_0 (J/m^2)	A (MPa)	S (N/mm)	D (mm)	t_f^{ID}	p_m^f (MPa)	K_{IC} (MPa m$^{1/2}$)
Value	210	0.3	0.165	618.95	1.927	1950	613.8	4628.9	2.5	1.92	1449.16	66.13

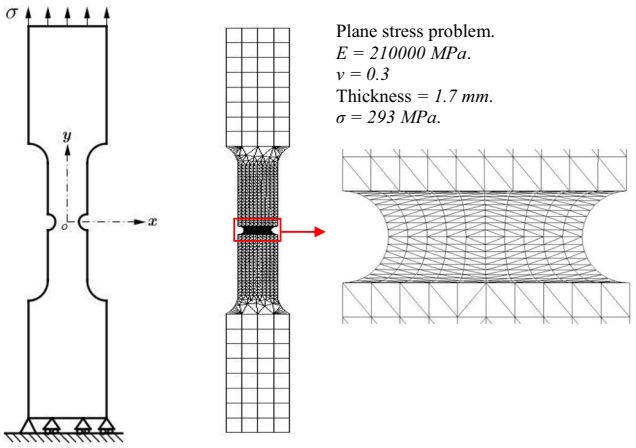

Fig. 9 "Franc2D" geometry model and the applied mesh 2-mm grooved specimen

where R is the curvature radius after fracture at the neck of the damaged zone, and r is the half width of the specimen after fracture at the neck.

The fracture strain ε_f can be calculated using Eq. (14) [23]:

$$\varepsilon_f = \sqrt{2/3}\sqrt{\varepsilon_{xx}^2 + \varepsilon_{yy}^2 + \varepsilon_{zz}^2} \tag{14}$$

As the tensile specimen is flat, the deformations in the three directions—ε_{xx}, ε_{yy}, and ε_{zz}—can be calculated through Eqs. (15)–(17):

$$\varepsilon_{xx} = \ln\left(\frac{w}{w_0}\right) \tag{15}$$

$$\varepsilon_{yy} = ln\left(\frac{t}{t_0}\right) \tag{16}$$

And as

$$\varepsilon_{xx} + \varepsilon_{yy} + \varepsilon_{yy} = 0 \Rightarrow \varepsilon_{zz} = -\left(\varepsilon_{xx} + \varepsilon_{yy}\right) \tag{17}$$

w_0 and w are the initial width and final width of damaged zone in the tensile specimen.

t_0 and t are the Initial thickness and final thickness of damaged zone in the tensile specimen.

The respective values of r, R, and t_f at the neck of the specimen for the 4 initial R_i (R_2, R_4, R_{10}, and R_{80}) are given in Table 6. The final widths and thicknesses together with the corresponding fracture strain are given in Table 7:

So, a plot of fracture strains to stress triaxiality permits determining the relationship between the fracture strain (ε_f) and stress triaxiality (t_f) from the equation of the fitting curve (Fig. 8).

The values of the parameters λ and α in Eqs. (7) and (9) are then, respectively, 0.754 and 2.3254.

So, the values of stress triaxility for indentation deformation (t_f^{ID}) and critical mean contact pressure (p_m^f) are calculated by Eqs. (7) and (8): t_f^{ID} = 1.92 and p_m^f = 1449.16 MPa.

4.3 Fracture toughness from IEF model

The fracture toughness value of the galvanized E26 steel sheet is hence determined by introducing the values of the parameters in Eq. (2). Table 8 summarizes the corresponding

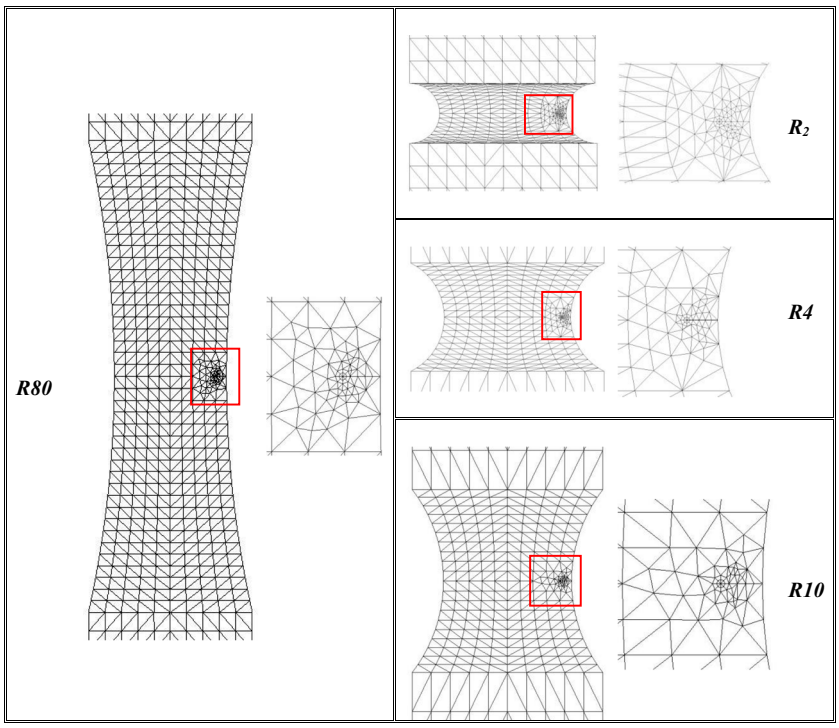

Fig. 10 Meshing of the crack with "Franc2D" from four grooved specimen (R_2, R_4, R_{10}, and R_{80})

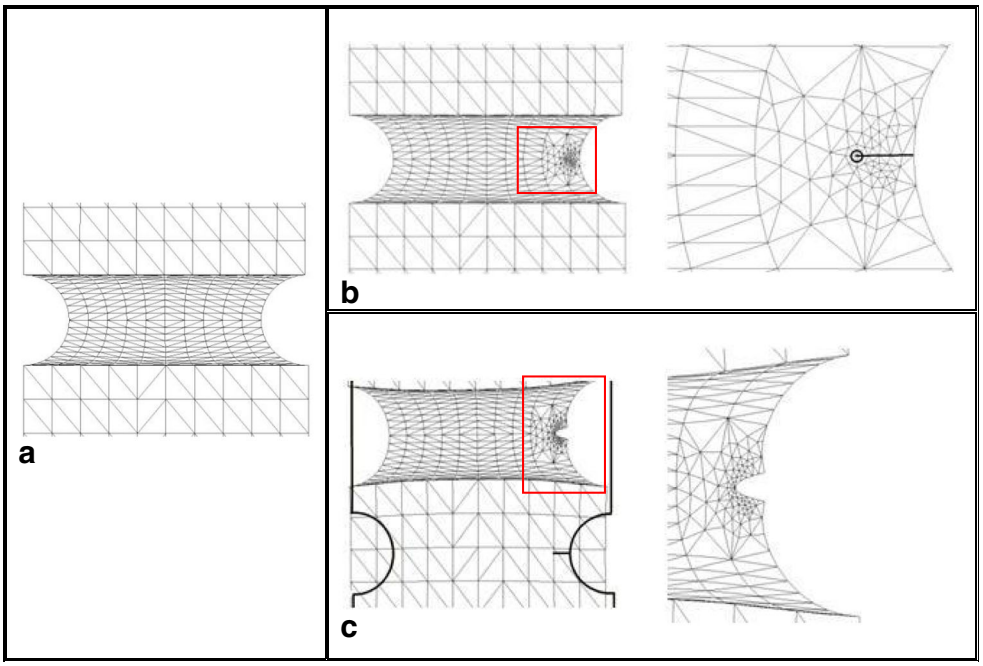

Fig. 11 **a** Mesh before simulation for a 2-mm grooved specimen. **b** Simulation results on non-deformed mesh. **c** Simulation results on deformed mesh

parameters used in the IEF model and calculated value of the fracture toughness of the galvanized E26 steel sheet.

5 Numerical model for K_{IC} determination

The numerical model for the determination of K_{IC} is based on developed by the Cornell Fracture Group from Cornell University, USA (http://www.cfg.cornell.edu/). The use of Franc2D software for modeling fracture of materials has been adapted for more than 20 years [24–29]. In the present work, the procedure of evaluating the fracture toughness of the material followed the procedure described in the literature [30–32].

Basically, the procedure suggests ten steps:

1. Create of the geometrical model of a tensile specimen, through "CASCA" software [33] distributed with Franc2D.
2. Generate the mesh of the geometrical model with the facilities of CASCA software.

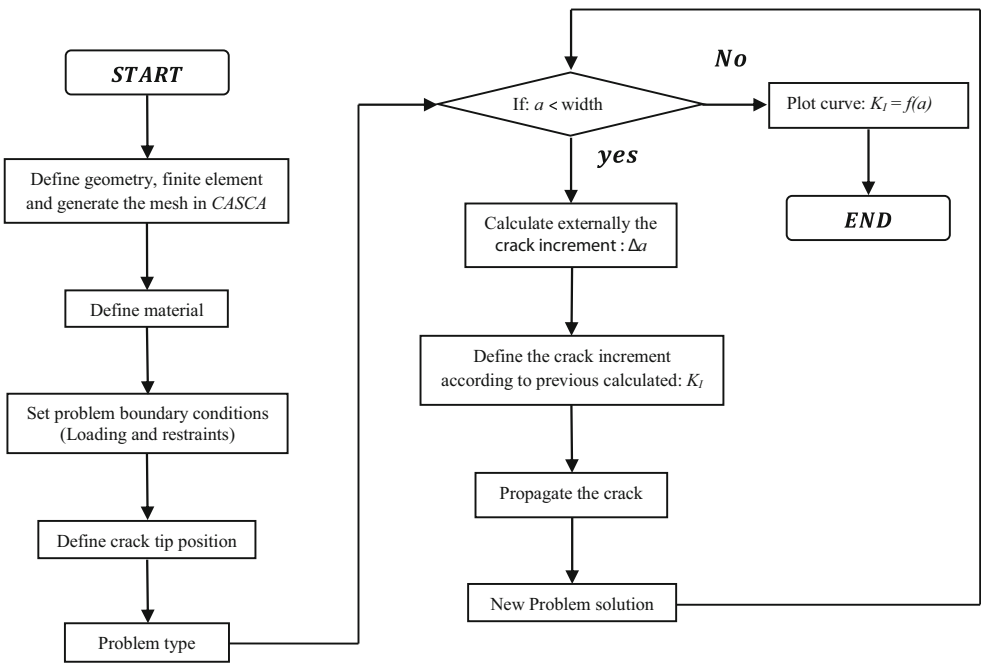

Fig. 12 Diagram of crack propagation approach in "Franc2D"

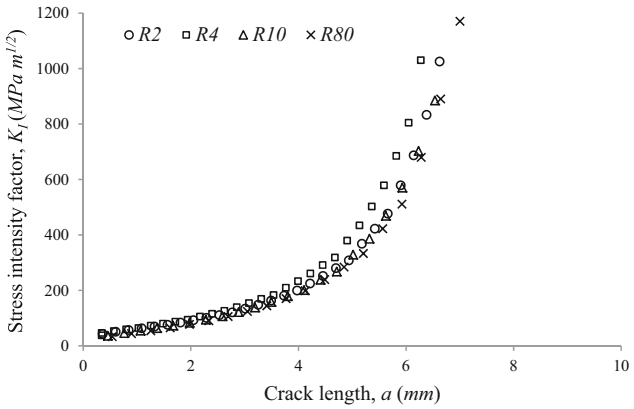

Fig. 13 Stress intensity factor to crack length curves as a function of the specimen groove radius

3. Set plane stress conditions to solve using the solutions of Franc2D software. Figure 9 shows the geometry model and corresponding mesh.
4. Input the mechanical properties (from smooth specimen tensile test results).
5. Set boundary and restrains conditions.
6. Set the loading conditions as to get the deformation of the material.
7. Create a crack that should be moving while simulating the tensile test. Figure 10 shows the results of the meshing of the crack zone as a function of the radius of the specimen groove before carrying out the tensile test simulation. Figure 11 illustrates simulation results.
8. Compute and get the stress intensity factor plot as a function of the moving crack using the diagram of crack propagation approach of Franc2D. The respective iterative calculation is given in the diagram illustrated in Fig. 12.
9. The procedure is repeated to the four grooved specimens (R_2, R_4, R_{10}, and R_{80}).
10. Determine the fracture toughness (K_{IC}) from the fitting curves of the stress intensity factor (K_I) to crack length (a) plots through mathematical solvers.

The plots of the stress intensity factor (K_I) versus the crack length for the four radii of grooved specimen are presented in Fig. 13. Using mathematical software "GeoGebra," the fitting curves are characterized by a polynomial function, Eq. (18), of order 7. Table 9 summarizes the respective constants as a function of the radius of the grooved specimens.

$$K_I = f(a) \tag{18}$$

The critical values of the crack length as a function of the specimen groove radius is obtained from the inflection point of the curve when the value of the second derivative of K_I is equal to 0, Eq. (19):

$$\frac{d^2K_I}{da^2} = 0 \tag{19}$$

Solving Eq. (18), when the crack length reaches its critical value (a_c), then the stress intensity factor gets its critical value corresponding to the fracture toughness. Then, the respective values (K_{IC}), as a function of the radius of the groove in the specimen, are given in Table 11.

Table 9 Constants of the polynomial functions for the values of the specimen groove radius

Groove radius	$K_I = f(a)$
R_2	$0.02\,a^7 - 0.32\,a^6 + 2.5\,a^5 - 10.7\,a^4 + 28.04\,a^3$–$39.91\,a^2 + 53.33\,a + 28.44$
R_4	$0.17\,a^7 - 3.37\,a^6 + 32.2\,a^5 - 142.78\,a^4 + 345.58\,a^3 - 440.81\,a^2 + 293.68\,a - 19.55$
R_{10}	$0.13\,a^7 - 3.02\,a^6 + 28.62\,a^5 - 139.49\,a^4 + 371.92\,a^3 - 526.84\,a^2 + 384.87\,a - 61.51$
R_{80}	$0.17\,a^7 - 4.26\,a^6 + 43.31\,a^5 - 227.39\,a^4 + 655.81\,a^3 - 1009.21\,a^2 + 776.42\,a - 181.03$

Table 10 Critical values of the crack length as a function of the specimen groove radius

Groove radius	Second derivative of $K_I = d^2K_I/da^2$	a_c (mm)
R_2	$(21/25)\,a^5 - (48/5)\,a^4 + 50\,a^3 - (642/5)\,a^2 + (4206/25)\,a - 79.82$	0.955
R_4	$(357/50)\,a^5 - (1011/10)\,a^4 + 644\,a^3 - (42{,}834/25)\,a^2 + (51{,}837/25)\,a - 881.62$	0.885
R_{10}	$(273/50)\,a^5 - (453/5)\,a^4 + (2862/5)\,a^3 - (4187/25)\,a^2 + (55{,}788/25)\,a - 1053.62$	1.035
R_{80}	$(357/50)\,a^5 - (639/5)\,a^4 + (4331/5)\,a^3 - (68{,}217/25)\,a^2 + (196{,}743/50)\,a - 2018.42$	1.134

Table 11 K_{IC} results from numerical solution

Groove radius	a_c (mm)	K_{IC} (MPa $m^{1/2}$)
R_2	0.956	60.13
R_4	0.886	62.84
R_{10}	1.035	55.20
R_{80}	1.134	53.60

Finally, the critical stress intensity factor (K_{IC}) corresponding to fracture toughness is calculated. The values are summarized in the Table 11.

6 Discussions

In the present work, a numerical method based on Franc2D software has been used to determine the K_{IC} of galvanized E26 steel sheets. Basically, the procedure followed ten steps from the creation of the geometrical model to the determination of K_{IC}. First, the evolution of the stress intensity factor (K_I) versus the crack length is simulated until the length of the crack reached about 75% of the whole width of the specimen. Then, a fitting curve is associated to extrapolate the corresponding equation expressing K_{IC} as a function of crack length, Eq. (18) and Table 9. The critical crack length (a_c) is obtained from the inflection point of the equation of the fitting curve when the value of the second derivative of K_I is equal to 0 (Table 10). Finally, from the critical crack length (a_c), the fracture toughness (K_{IC}) is calculated. The effect of the groove radius is shown in Table 11. The value of K_{IC} decreases when the groove radius, R, increases. This is caused by the stress concentration at the crack tip. In fact, when R is small, the gauge length of the specimen is 12.5 mm width with a notch length of 2.16 mm. The latter value corresponds to a semicircular groove of 2 mm and a fine crack initiation of 0.16 mm. As the groove radius increases, the gauge length decreases in width; therefore, the notch becomes smaller than 2.16 mm. In fact, at the end, for a groove radius of 80 mm, the width of the gauge length becomes 8.5 mm and the notch length is the initiated crack that is 0.16 mm. This is in good agreement of the phenomena observed in sharp cracks: the sharper the crack, the higher the value of fracture toughness. Figure 14 shows the illustration of stress distribution in the Y-axis for a 2-mm groove radius. When the specimen is stretched, there is a rotation around the crack tip creating compressive zone while the crack is propagating. In fact, the elastic stress of the material has already doubled and even overpasses the value of the ultimate stress of the material. By the time the blue color changes into cleared color the crack has already increased. In the red zone of the simulation results, the values indicate that damage has occurred. Figure 15 shows the simulation of the trajectory

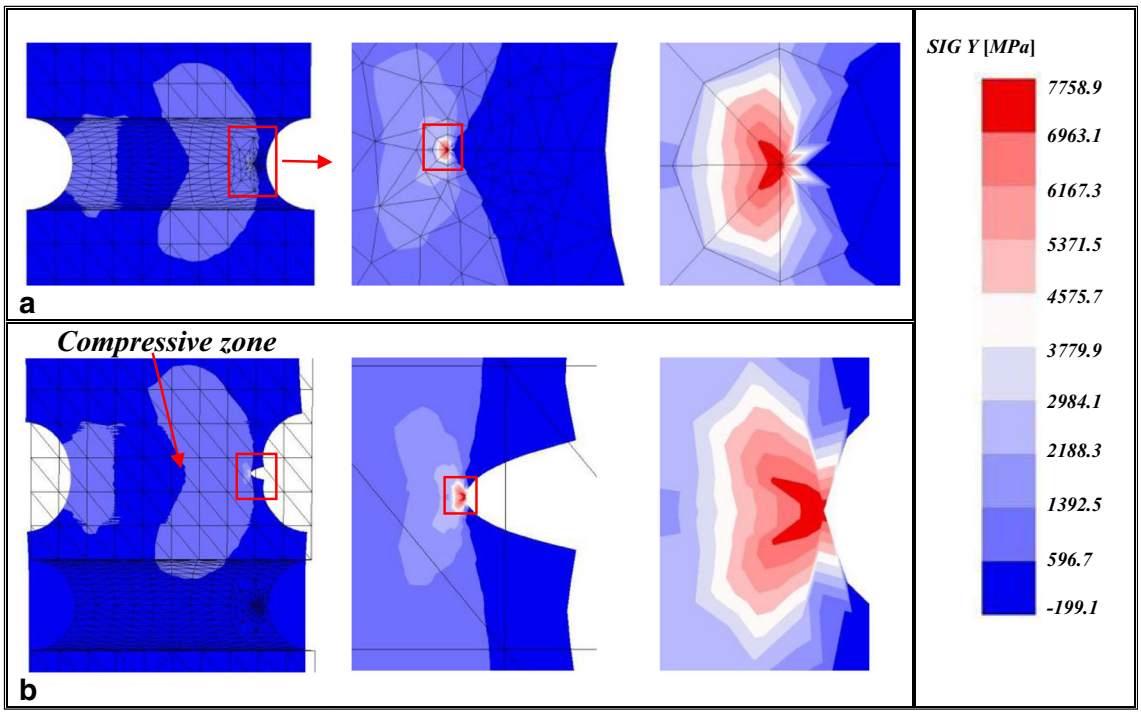

Fig. 14 Simulation of stress distribution SIG Y (MPa) in the 2-mm grooved specimen. **a** Non-deformed mesh. **b** Deformed mesh

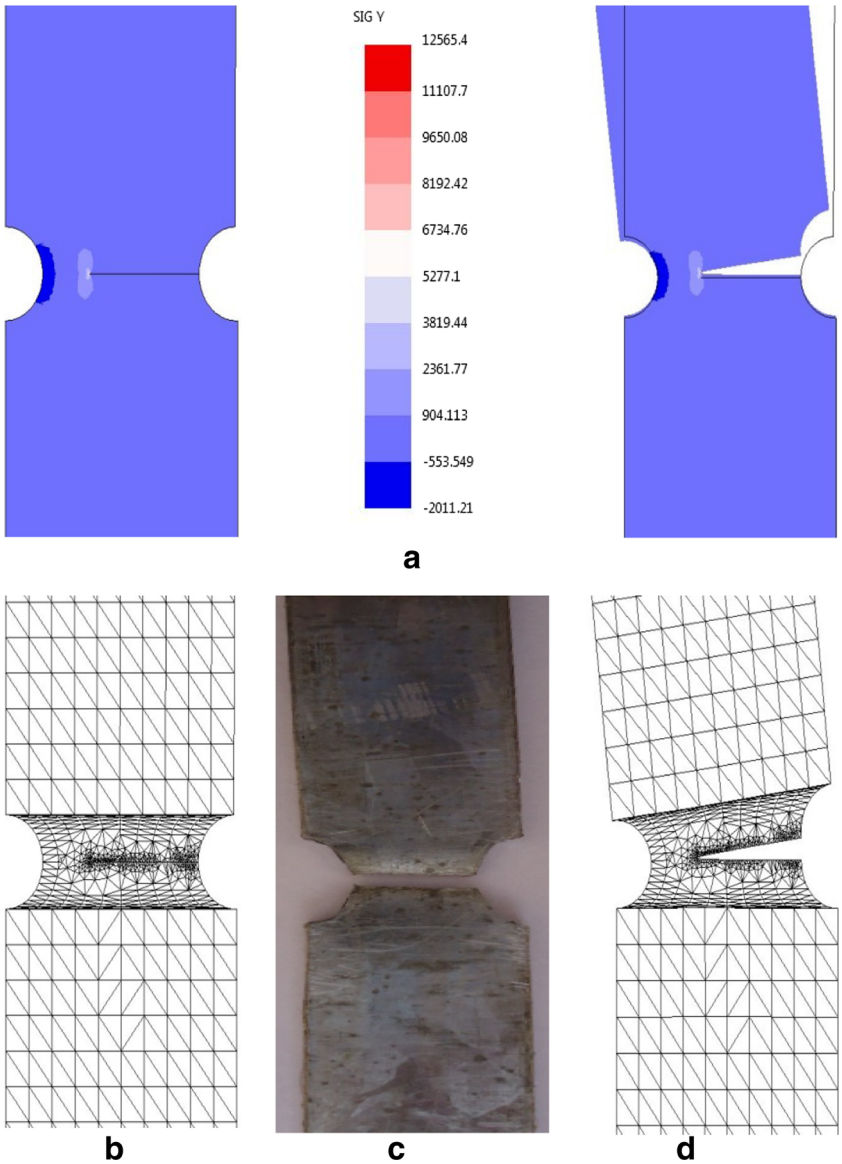

Fig. 15 **a** Stress distribution SIG *Y* (ksi) to failure and crack trajectory propagation in the 2-mm grooved specimen. **b** Non-deformed mesh to failure and crack trajectory propagation in the 2-mm grooved specimen. **c** Experimental crack trajectory propagation to failure for 2-mm grooved specimen. **d** Deformed mesh to failure and crack trajectory propagation in the 2-mm grooved specimen

of the crack propagation in the 2 mm grooved specimen in good agreement with that obtained experimentally.

In order to validate the numerical results, IEF model based on Vickers hardness tests results and its stress triaxiality factor is applied. For every mechanical testing, IEF method requisitions test machines, measuring equipment, data acquisition systems, know-how and machine operators and it also needs to prepare the corresponding specimens. The number of specimens depends on the experimental design and also on the reproducibility of the results through a series of at least three to five specimens. So, despite the great effort spent in improving the technology of the mechanical testing systems, experimental procedure remains time consuming, costly, and often implies uncertainties due to errors of operators and equipments. Fracture toughness has been computed using Eq. (2).

The results of fracture toughness values obtained from both methods IEF model and Franc2D solutions are presented in Table 12. Results of K_{IC} are in good agreement with a maximum coefficient of variation of 14%. For small groove radii, 2 and 4 mm, numerical and analytical results were 5 to 10% closer. When the groove radius becomes larger, the coefficient of variation increases almost to 20% because plane stress is relevant for grooves of small radius, the acceptable mean value of K_{IC} for galvanized E26 steel sheet is 63 MPa $m^{1/2}$. Thus, instead of wasting time in costly experimental tests, the use of Franc2D seems to be a good tool for determining the fracture toughness of materials. In addition, learning Franc2D was not so difficult especially for those who are accustomed to the finite elements computing software.

Table 12 Comparison between experimental solution and numerical solution

Model			
Groove radius	Numerical solution "Franc2D" K_{IC} (MPa $m^{1/2}$)	Experimental solution "IEF model" K_{IC} (MPa $m^{1/2}$)	Coefficient of variation (%)
R_2	60.13	66.13	10.0
R_4	62.84		05.2
R_{10}	55.20		19.8
R_{80}	53.60		23.4
Average	57.94	66.13	14.1

7 Conclusion

In the present work, a numerical approach based on the derivation method of Bridgman is proposed to determine K_{IC} of galvanized E26 steel sheets using a free fracture analysis numerical code, Franc2D. Basically, the concept of the software is simple and focuses on linear fracture mechanics analysis where the crack growth is simulated from initiation to final fracture. From simulations of tensile test of different geometrical models of notched specimen gauge length, plots of the stress intensity factor (K_I) versus the crack length are therefore easily obtained and then explored in order to determine the fracture toughness (K_{IC}) of the material through common mathematical transformations. The results are then compared to those obtained by an experimental approach using IEF model based on Vickers hardness tests results and the determination of stress triaxiality factor of the material. Series of standard tensile tests on smooth and grooved specimens were required to conduct the investigation.

Results of K_{IC} in galvanized E26 steel sheet were reasonably in good agreement, and a mean coefficient of variation of 14% has been observed for different radius grooved specimens. For smaller groove radius, numerical results were the closer and acceptable. For high groove radius of 80 mm, the maximum coefficient of variation was about 20%. Hence, the mean value of K_{IC} is 63 MPa $m^{1/2}$ is derived from small groove radius. The proposed numerical approach can be used for determining fracture toughness in galvanized metal sheets.

Acknowledgements The authors are very grateful to the steel complex El-Hadjar, Algeria, for machining the specimens and chemical analysis of the material. Special thanks to Cornell Fracture Group from Cornell University, USA, to let free software for scientific research. Financial supports are due to laboratories LRTAPM and LR3MI of Badji Mokhtar University, Annaba, Algeria, under the direction of *DGRSDT*, Algeria, and through the project code CSCU232010 (www.dgrsdt.dz).

References

1. Coni N, Gipiela ML, D'Oliveira ASCM, Marcondes PVP (2009) Study of the mechanical properties of the hot dip galvanized steel and galvalume. J of the Braz Soc of Mech Sci and Eng 4:319–326
2. Seré PR, Culcasi JD, Elsner CI, Di Sarli AR (1999) Relationship between texture and corrosion resistance in hot-dip galvanized steel sheets. Surf Coat Technol 122:143–149
3. Cheng JG, Zhang J, Chu CC, Zhe J (2005) Experimental study and computer simulation of fracture toughness of sheet metal after laser forming. Int J Adv Manuf Technol 26:1222–1230
4. Shih HC, Hsu JW, Sun CN, Chung SC (2002) The lifetime assessment of hot-dip 5% Al-Zn coatings in chloride environments. Surf Coat Technol 150:70–75
5. Carbucicchio M, Ciprian R, Ospitali F, Palombarini G (2008) Morphology and phase composition of corrosion products formed at the zinciron interface of a galvanized steel. Corros Sci 50:2605–2613
6. Hayat F, Sevim I (2012) The effect of welding parameters on fracture toughness of resistance spot-welded galvanized DP600 automotive steel sheets. Int J Adv Manuf Technol 58:1043–1050
7. Asgari A, Toroghinejad MR, Golozar MA (2009) Effect of coating thickness on modifying the texture and corrosion performance of hot-dip galvanized coatings. Curr Appl Phys 9:59–66
8. Kim H, Sung J, Goodwin FE, Altan T (2008) Investigation of galling in forming galvanized advanced high strength steels (AHSSs) using the twist compression test (TCT). J Mater Process Technol 205:459–468
9. Ploypech S, Boonyongmaneerat Y, Jearanaisilawong P (2012) Crack initiation and propagation of galvanized coatings hot-dipped at 4500C under bending loads. Surf Coat Technol 206: 3758–3763
10. Lai WJ, Pan J (2014) Stress intensity factor solutions for adhesive-bonded lap-shear specimens of magnesium and steel sheets with and without kinked cracks for fatigue life estimations. Eng Fract Mech 131:454–470
11. Byun TS, Kim SH, Lee BS, Kim IS, Hong JH (2000) Estimation of fracture toughness transition curves of RPV steels from ball indentation and tensile test data. J Nucl Mater 277:263–273
12. Byun TS, Kim JW, Hong JH (1998) A theoretical model for determination of fracture toughness of reactor pressure vessel steels in the transition region from automated ball indentation test. J Nucl Mater 252:187–194
13. Haggag FM, Byun TS, Hong JH, Miraglia PQ, Murty KL (1998) Indentation-energy-to-fracture (IEF) parameter for characterization of DBTT in carbon steels using nondestructive automated ball indentation (ABI) technique. Scripta Matetialia 38(4):645–651

14. Khandelwal HK, Sharma K, Chhibber R (2012) Mechanical property estimation of similar weld using ball indentation technique. J Miner Mater Charact Eng 11:1095–1100
15. Mohammadi AH, Naderi M, Iranmanesh M (2011) Fracture toughness evaluation of 3Cr-1Mo steel from Vickers indentation and tensile test data. Procedia Engineering 10:228–235
16. Bridgman PW (1952) Studies in large plastic flow and fracture. McGraw-Hill.
17. Bai Y (2008) Effect of loading history on necking and fracture. PhD thesis, Massachusetts Institute of Technology, USA
18. Holloman JH (1945) Tensile deformation. Trans AIME 162:268–290
19. ASTM E1921-98 (1998) Test method for the determination of reference temperature, T_0, for ferritic steels in the transition range
20. Moussa C, Bartier O, Mauvoisin G, Delattre G, Hernot X (2013) Revue bibliographique sur la caractérisation mécanique des matériaux utilisant la déformation représentative en indentation sphérique. Matériaux et technique 101:302
21. Bektes M, Uzun O, Akt rk S, Ekinci AE, Uçar N (2004) Vickers Microhardness studies of Fe-Mn binary alloys. Chin J Phys 42(6): 733–739
22. Davis JR (2004) Tensile testing, second edition. ASM International 13:226–227
23. Kut S (2010) A simple method to determine ductile fracture strain in a tensile test of plane specimens. Metalurgija 49(4):295–299
24. Dzik EJ, Lajtai EZ (1996) Primary fracture propagation from circular cavities loaded in compression. Int J Fract 79:49–64
25. Cendon DA, Galvez JC, Elices M, Planas J (2000) Modelling the fracture of concrete under mixed loading. Int J Fract 103:293–310
26. Carpinteri A, Invernizzi S (2005) Numerical analysis of the cutting interaction between indenters acting on disordered materials. Int J Fract 131:143–154
27. Lim WK (2011) Determination of second-order term coefficients for the inclined crack in orthotropic plate using singular finite elements. Int J Fract 168:125–132
28. Seifi R, Eshraghi M (2013) Effects of mixed-mode overloading on the mixed-mode I + II fatigue crack growth. Arch Appl Mech 83: 987–1000
29. Al-Mukhtar AM (2016) Mixed-mode crack propagation in cruciform joint using Franc2D. J Fail Anal And Preven, Tools and techniques, CrossMark
30. Wawrzynek P, Ingraffea A (1994) Franc2D: a two-dimensional crack propagation simulator. Tutorial and User's Guide, Version 2.7, NASA contractor report 4572
31. Iesulauro E (1995) Franc2D/L A crack propagation simulation for plane layered structures. Version 1.5 user's guide. Cornell University, Ithaca, New York
32. Iesulauro E (2002) Franc2D/L A crack propagation simulator for plane layered materials. Cornell University, Ithaca, New York
33. Wawrzynek P, Martha L (1997) CASCA: a simple 2-D mesh generator, version 1.4 user's guide. Cornell University, Ithaca, New York